AGU ADVANCING EARTH AND SPACE SCIENCES

Geophysical Research Letters

RESEARCH LETTER
10.1029/2024GL111775

The 2022 February 15 Solar Energetic Particle Event at Mars: A Synergistic Study Combining Multiple Radiation Detectors on the Surface and in Orbit of Mars With Models

Jian Zhang[1,2], Jingnan Guo[1,3], Yongjie Zhang[4], Yihang Cao[1], Mikhail I. Dobynde[1], Cunhui Li[1,5], Yuhong Yu[4], Yuming Wang[1], Shuwen Tang[4], Yi Qian[4], Hongyun Zhao[4], Zhiyu Sun[4], Yi Wang[5], and Robert F. Wimmer-Schweingruber[6]

[1]Deep Space Exploration Laboratory/School of Earth and Space Sciences, University of Science and Technology of China, Hefei, China, [2]Department of Physics and Astronomy, University of Turku, Turku, Finland, [3]Collaborative Innovation Center of Astronautical Science and Technology, Harbin, China, [4]Institute of Modern Physics, Chinese Academy of Sciences, Lanzhou, China, [5]Science and Technology on Vacuum Technology and Physics Laboratory, Lanzhou Institute of Physics, Lanzhou, China, [6]Institute of Experimental and Applied Physics, Christian-Albrechts-University, Kiel, Germany

Key Points:

- A major solar particle event (SPE) was simultaneously measured by multiple detectors both on the surface and in orbit of Mars
- The first analysis of a SPE at Mars measured by the Tianwen-1 Mars orbiter serves to verify its capacity in high-energy particle detection
- We compare the radiation measurements, both on the surface and in orbit of Mars, with results derived from data-based models

Correspondence to:

J. Guo, Y. Zhang, C. Li and Z. Sun,
jnguo@ustc.edu.cn;
zhangyj@impcas.ac.cn;
licunhui@spacechina.com;
sunzhy@impcas.ac.cn;

Citation:

Zhang, J., Guo, J., Zhang, Y., Cao, Y., Dobynde, M. I., Li, C., et al. (2024). The 2022 February 15 solar energetic particle event at Mars: A synergistic study combining multiple radiation detectors on the surface and in orbit of Mars with models. *Geophysical Research Letters*, *51*, e2024GL111775. https://doi.org/10.1029/2024GL111775

Received 2 AUG 2024
Accepted 25 SEP 2024

Abstract On 2022-02-15, solar eruptions caused one of the most intensive Solar Particle Events (SPEs) in Solar Cycle 25 observed at various heliospheric locations. This study focuses on the enhancements of energetic proton flux observed by multiple detectors located at the orbit and on the surface of Mars. We carry out the first analysis by the Mars Energetic Particle Analyzer (MEPA) instrument on board the Chinese Tianwen-1 spacecraft (TW-1) at Mars orbit which also serves to validate the instrument's capability to measure protons of up to 100 MeV. We reconstruct the event spectrum up to 1 GeV and further model the event doses at Mars's orbit and surface which are then validated against the corresponding dosimetry data. Our study utilizes all available radiation detectors at Mars, advances our understanding of Mars's radiation environment induced by large SPEs, and emphasizes the necessity of continuous and synergistic radiation monitoring at Mars.

Plain Language Summary There is a growing interest in exploring Mars in the coming decades. However, a significant obstacle that remains is the presence of space radiation, which poses a considerable and unavoidable threat to crew health, especially during long-term stays in future Martian habitats. Of particular concern are sporadic energetic particle events caused by strong solar eruptions, which can increase radiation levels in deep space and near Mars to potentially dangerous levels. Notably, a SEP event on 15 February 2022 has caused the first significant radiation enhancement at Mars in Solar Cycle 25 as observed by ESA's Trace Gas Orbiter, Chinese Tianwen-1 orbiter as well as NASA's Mars Atmosphere and Volatile Evolution spacecraft and the Curiosity rover. By combining data from measurement and modeling techniques, we reconstruct the energy spectrum of this SEP event to understand the potential radiation hazards at Mars.

1. Introduction

Space radiation can affect humans as well as hardware and communications. A comprehensive understanding of space radiation is necessary for space exploration activities, especially for future crewed mission to Mars. Mars is significantly exposed to space radiation because of its thin atmosphere (of about 20 g/cm^2 of vertical column depth) and lack of a global intrinsic magnetic field. An increasing number of investigations on the Martian radiation environment have been conducted and a lot of progress has been made during the past decades. Particularly with the measurements by the Radiation Assessment Detector (RAD, Hassler et al., 2012) on board the Mars Science Laboratory (MSL, Grotzinger et al., 2012) since its landing on Mars in August 2012 (Zeitlin et al., 2013; Hassler et al., 2014; Guo et al., 2021, and references therein). Since 2014, proton fluxes from 20 keV to about 6 MeV can be obtained from the Solar Energetic Particle instrument onboard the Mars Atmosphere and Volatile Evolution (MAVEN/SEP) spacecraft (Larson et al., 2015) which has recorded many energetic particle events associated with solar eruptions or stream interaction regions at Mars (Lee et al., 2017). Most of these SEP events are not detected by MSL/RAD on the surface because the Martian atmosphere can slow down and even stop most energetic particles below about 150 MeV (e.g., Guo et al., 2018). In May 2018, ESA's ExoMars Trace Gas Orbiter (TGO) spacecraft was inserted to Mars's 400 km circular orbit and the Liulin-MO dosimeter on board has been conducting the orbital radiation dosimetry measurement since then (Semkova et al., 2021, 2022). Since 2021, the Chinese Tianwen-1 (TW-1) spacecraft has arrived at Mars and the Mars Energetic Particle Analyzer

(MEPA) instrument started recording the energetic particle flux including 2–100 MeV protons, and 25–300 MeV alpha particles and heavier ions (Fu et al., 2022; Li et al., 2021; Tang et al., 2020).

On 15 February 2022 a large Solar Energetic Particle (SEP) event occurred and was detected by multiple instruments at different radial distances and longitudinal locations in the inner heliosphere including Earth, Mars, STEREO-A, Parker Solar Probe (PSP) and Solar Orbiter (Figure 1b). This event was accompanied by a remarkable Coronal Mass Ejection (CME), which achieved a speed of > 2300 km/s at a heliocentric height of 25 solar radii (Khoo et al., 2024). The CME geometry reconstructed using the Graduated Cylindrical Shell model (GCS; Thernisien, 2011) and the coronagraph images obtained from the STEREO-A and SOHO spacecraft is depicted in Figure 1a by the green grid mesh. The nose of the CME is positioned at a longitude of $\sim 135°E$ and a latitude of $\sim 37°N$ in Stonyhurst coordinates, with an angular extent in the equatorial plane of $\sim 45°$ (estimated based on Dumbović et al., 2019). This particular event is not exactly directed toward Mars; however, its flank was probably magnetically connected to Mars (Figure 1b). This observation aligns with the significant rise in proton flux recorded by the detectors deployed both on the surface and at the orbit of Mars. PSP was magnetically connected to the leading edge of the CME. At the same time, the STEREO-A, Solar Orbiter, and Earth spacecraft were magnetically connected to the opposite side of the Sun and observed a gradual increase in proton flux (Figures 1c and 1d), likely attributed to the cross-field diffusion of particles.

This large SEP event accelerated particles to energies high enough to penetrate the Martian atmosphere. It is in fact the first event which allows synergistic analysis combining four different radiation detectors at Mars: MAVEN, TW-1, TGO in orbit and MSL on the surface. Similar to ground level enhancements on Earth (Mishev & Usoskin, 2019), we reconstruct the SEP energy spectrum from 1 MeV to 1 GeV by combining the response of the ground-based detector MSL/RAD to high-energy protons (>150 MeV) and the flux of protons ≤100 MeV measured by space-borne detectors TW-1/MEPA and MAVEN/SEP. For the first time, we provide the SEP spectra observed at Mars over such a large energy range. This advances our understanding of the properties and impact of large SEP events at Mars's distance.

In this letter, based on multi-spacecraft observations at Mars by MAVEN, TW-1, TGO in orbit and MSL on the surface, we reconstruct the energy spectrum of the 2022 February 15 SEP event at Mars (Section 2). We then utilize the reconstructed spectrum to calculate the radiation doses at Mars's orbit and surface which are then compared to the recorded doses by TGO/Liulin-MO and MSL/RAD detectors (Section 3). We discuss the reliability of TW-1/MEPA data and our method to extend the SEP spectrum up to about 1 GeV through a comparative analysis of simulated results and measured data. We stress the importance of continuous and synergistic radiation monitoring at Mars.

2. SEPs Arriving at Mars

2.1. Orbital and Surface Measurements

The significant impact of this event has unfortunately led to two temporary halts in functionality of the TW-1/MEPA instrument. Only 12 hr of data are available at the onset of the event, with an additional 12 hours of data during the decay phase, as shown in Figure 1d. MEPA is designed to measure proton flux in the energy range from 2 to 100 MeV and with limited communication bandwidth, only a subset of registered particles going through the MEPA detector are sent back and used to calculate energy deposition and particle spectra (Li et al., 2021; Tang et al., 2020). Due to the significance of this event and the unexpected interruption of the observation, the ratio of the sampled data to the total registered ones under 20 MeV is unusually low and unfortunately not precisely recovered. The big uncertainty of this ratio made the proton flux in this energy range unreliable which is therefore excluded from the following analysis. Nevertheless, the existing proton flux data ranging from 20 to 100 MeV can serve to reconstruct the energy spectrum during the onset period of the event (indicated by the gray-shaded areas in Figure 2a). This energy range is critical for studying the characteristics of SEP events since the break energy of the SEP double power-law spectrum normally locates within this range (Raukunen et al., 2018). Meanwhile, MAVEN/SEP provides a continuous measurement of the low-energy SEPs (below about 6 MeV) which complements the MEPA measurement at higher energies. As shown, the enhanced flux of low-energy SEPs at Mars lasts for days while the fluxes of high-energy channels ($> \sim 50$ MeV) mostly reached the peaks values within 12 hr after the SEP onset.

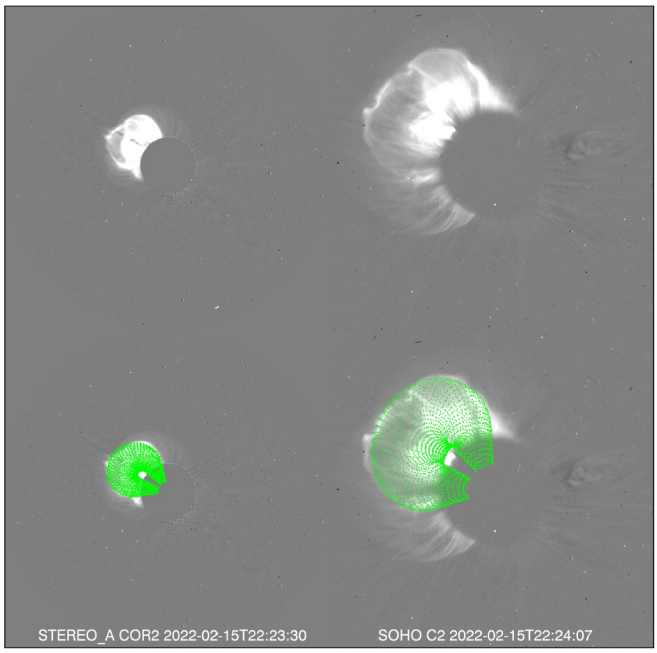

(a)

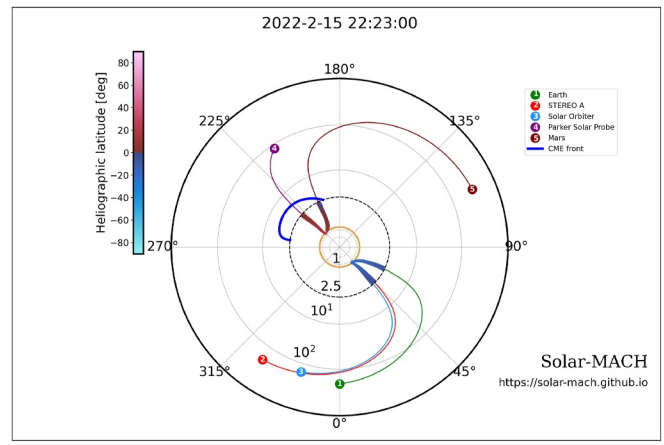

(b)

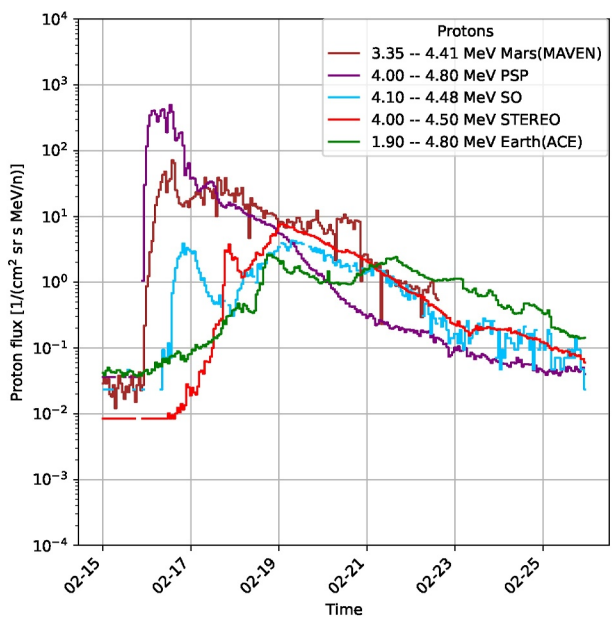

(c)

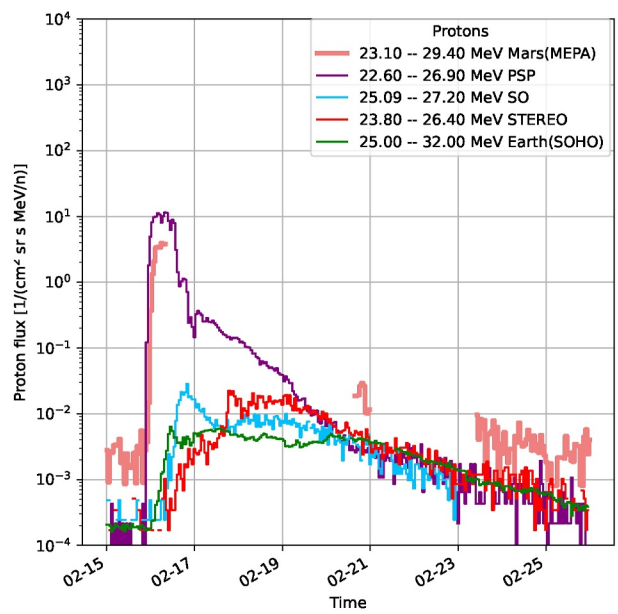

(d)

Figure 1. Overview of the 15–16 February 2022 SEP event. (a) GCS reconstruction of the CME using observations of STEREO-A/COR2 (left) at 22:23:30 and SOHO/LASCO/C2 (right) at 22:24:07. The fitted CME direction is $(135°E, 37°N)$; the tilt angle is $-75°$; the height is 6 AU, the ratio is 0.3; and the half angle is 30°. (b) Spacecraft's and planets' configuration in the inner Solar System on 15 February 2022, including PSP, Mars, Earth, STEREO-A, and Solar Orbiter. CME's front are shown in blue. Nominal interplanetary magnetic fields connecting each observer to the Sun are also plotted. The orbit plot is created with the Solar MAgnetic Connection HAUS (Solar-MACH; Gieseler et al., 2023). (c) The time profiles of ∼4 MeV proton intensities from different spacecraft with a time resolution of 1 hr. (d) The time profiles of ∼25 MeV proton intensities from different spacecraft with a time resolution of 1 hr.

Secondary back-scattered particles produced at the surface and atmosphere of Mars can make a small contribution $\sim 5-6\%$ to the orbital radiation as an albedo component (Liu et al., 2023; Semkova et al., 2022). Albedo particles cannot be directly distinguished by MEPA from those from deep space because the instrument has only one

10.1029/2024GL111775

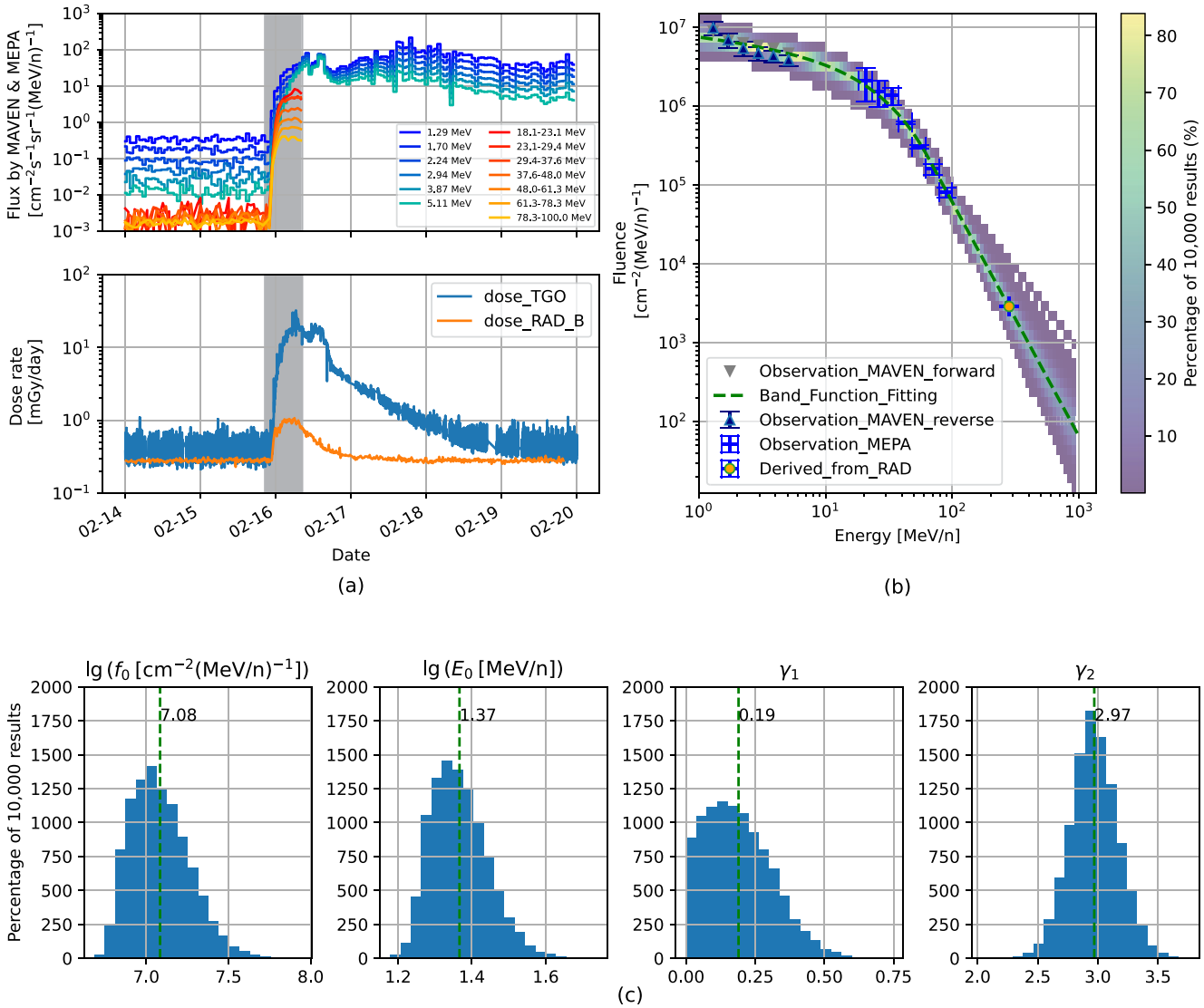

Figure 2. Flux, dose rate, and spectrum of the SEP event at Mars. (a) The proton flux measured by MAVEN/SEP (sensor 1, reverse direction) and TW-1/MEPA detectors (upper panel) and the dose rates measured by TGO/Liulin-MO "AB" detector pairs and the MSL/RAD "B" detector (lower panel). (b) Reconstructed spectra of the SEP event based on various datasets (MAVEN, MEPA and RAD) at Mars integrated for the initial 12 hr after the event onset as shaded in (a). The shaded area in (b) shows the percentage of 10,000 results of Band function fitting and the green dashed line represents the Band function using the mean values of parameters. (c) The distribution of the Band function parameters based on 10,000 fits and the final mean values of parameters (the green vertical dashed lines). More details can be found in the main text of Section 2.

viewing direction. During this event, MEPA was facing away from Mars with minimal contribution by the Martian albedo particle flux and also approximately pointing at the opposite direction of the Sun. During the very beginning of the SEP events when most particles arrive along the interplanetary magnetic field lines and the anisotropy of the event is high, the flux measured by MEPA may be lower than the forward-looking (at the Sun) direction. For lower-energy particles measured by MAVEN, we are able to probe the flux directionality. As shown in Figure 2b which will be explained in detail in Section 2.3, the fluence measured in the forward direction (with respect to the Sun) of the MAVEN/SEP sensor one instrument (gray down-pointing triangles) is about 20% larger than that in the reverse direction (blue up-pointing triangles). Nevertheless, to keep the consistency of the orbital measurements, we use the MAVEN data in the reverse direction for the following analysis. On the other hand, the local time of MSL/RAD on the surface was 3 a.m. at the onset of the event and was around noon during the event peak time. It means that MSL/RAD was detecting particles from the Solar direction during the main phase of the event.

Figure 2a shows that during the event and especially during the initial phase, the radiation levels, here quantified as the absorbed dose rate in silicon recorded in the TGO/Liulin-MO and MSL/RAD silicon detectors, have increased significantly both in orbit of Mars and on its surface. The surface dose rate is about 10 times lower than the orbital dose rate and the duration of its enhancement is also shorter. This is because more low-energy SEPs with a higher flux and longer duration can contribute to the orbital radiation, but they are easily absorbed by the Martian atmosphere.

Comparing the time evolution of particle fluxes and dose rates in Figure 2a, we note that low-energy SEPs measured by MAVEN/SEP show a different time evolution than the dose rate. So these low-energy SEPs should have small impact on the dose rate measured, while SEPs with energies recorded by MEPA or even above contribute more to radiation doses. For the orbital dose measurement, this may be related to the shielding of the TGO spacecraft (detailed and investigated below in Section 3.1) which can effectively stop protons $<\sim$10 MeV from reaching the TGO dosimeter. For the surface measurement, only protons with energies above about 150 MeV can arrive at the surface due to the atmospheric shielding (more details in Section 2.2). Therefore, for evaluating the radiation effect of SEPs, it is critical to reconstruct the complete SEP energy spectrum and quantify its contribution to dose, as has been carried out in this study.

2.2. The Martian SEP Pivot Energy

Due to the atmospheric shielding effect, the surface MSL/RAD detector actually responds to incoming SEP protons with energies above about 150 MeV. Exploiting this feature, we can use the Martian atmosphere as a "high-energy particle absorber" to derive the primary SEP flux at higher energies. Using particle-atmosphere interaction models, the research by Guo, Wimmer-Schweingruber et al. (2019) modeled Martian surface radiation levels caused by 72 large SEPs with single power-law spectra and found a strong correlation between the radiation dose [mGy/hour] on the surface of Mars (with a pressure of about 800 Pa) and the SEP proton flux [particles s^{-1} sr^{-1} cm^{-2} MeV^{-1}] at an energy of 300 MeV which was referred to as the pivot-energy. The correlation is described as follows:

$$D_{\mathrm{Mars}} = 4.45 \cdot I_{300MeV}, \tag{1}$$

where D_{Mars} is the radiation dose on the surface of Mars; $I_{300\mathrm{MeV}}$ is the proton flux at 300 MeV pivot energy. They are linearly correlated by the coefficient 4.45. Subsequent studies have further confirmed the presence of pivot-energy of SEP events characterized by double power-law spectra and showed that the pivot energy is not always 300 MeV and varies in response to variations of the Martian surface atmospheric pressure (Zhang et al., 2023).

The pivot-energy correlation has strong application aspects. The first is that one can estimate the surface dose rate $\mathrm{D_{Mars}}$ directly from the SEP flux at this energy without knowing other spectral properties such as the power-law index. The other is that one can also derive the primary proton flux at this energy F_p from the surface dose measurement by MSL/RAD, which is $\mathrm{D_{Mars}}$. The latter method is used in this study with the correlation equations as derived by Zhang et al. (2023, Figure 7). This study found that both the pivot energy, E_p, and the linear correlation factor, C_p (between the surface dose measured by RAD, D_{Mars}, and the fluence, F_p at the pivot energy) have a dependence on the surface pressure p following the quadratic empirical functions.

$$E_p = a_1 \cdot p^2 + b_1 \cdot p + c_1, \tag{2}$$

$$C_p = a_2 \cdot p^2 + b_2 \cdot p + c_2, \tag{3}$$

$$F_p = \frac{D_{\mathrm{Mars}}}{C_p}, \tag{4}$$

The coefficients a_1, b_1, c_1, a_2, b_2, and c_2 are given in Zhang et al. (2023). The methodology implementation and uncertainty estimations are detailed in the next subsection.

2.3. SEP Spectra and Uncertainty Estimation

We adopt the commonly used Band function (Band et al., 1993) to fit the SEP spectrum at Mars combining the MAVEN and MEPA data together with the derived fluence at the pivot energy assuming that the SEP flux ranges up to 1 GeV. To evaluate the uncertainty of the fitting results which may originate from the surface pressure changes and measurement uncertainties of MAVEN and MEPA, we use a Monte Carlo method that involves the following steps.

1. Randomly select the surface pressure P following $P \sim N(\bar{p},\sigma_p^2)$, where N is the Gaussian distribution, and $\bar{p}$ is the average Martian surface atmospheric pressure during this event. As measured by the Mars Science Laboratory Rover Environmental Monitoring Station, $\bar{p}$ is 729 Pa and σ_p is 29 Pa from 22:00 on February 15 to 8:00 on 16 February 2022.
2. Randomly select the coefficient of Equation 2, $\mathbf{COEF_1} \sim \mathcal{N}(\langle\mathbf{COEF_1}\rangle,\mathbf{\Sigma_{COEF_1}})$, the coefficient of Equation 3, $\mathbf{COEF_2} \sim \mathcal{N}(\langle\mathbf{COEF_2}\rangle,\mathbf{\Sigma_{COEF_2}})$, where $\mathbf{COEF_1} = [a_1,b_1,c_1]$, $\mathbf{COEF_2} = [a_2,b_2,c_2]$. $\mathcal{N}$ is the multivariate Gaussian distribution. The mean, $\langle\mathbf{COEF_1}\rangle$, $\langle\mathbf{COEF_2}\rangle$ and covariance, $\mathbf{\Sigma_{COEF_1}}$, $\mathbf{\Sigma_{COEF_2}}$ are obtained by fitting E_p and C_p that vary with surface pressure using a quadratic function (Equations 2–4 and more details in Zhang et al., 2023).
3. Calculate the values of E_p, C_p and F_p using the randomly selected parameter from steps 1 and 2 according to Equations 2–4. The mean value of E_p equals to 278 MeV (lower than 300 MeV for Equation 1 since the surface pressure considered here is lower than that for Equation 1) and the mean value of C_p equals to 3.86 (mGy h^{-1})/(particles s^{-1} sr^{-1} cm^{-2} MeV^{-1}), which is ∼13% smaller than the 4.45 in Equation 1. Note that the surface doses under these two pressure conditions, for the same SPE spectrum, would have a difference much smaller than 13% since the flux at 300 MeV is smaller than that at 278 MeV.
4. Further consider errors of the measurement. We use f_{obs} representing the measured fluence for 12 hr (the gray region shown in Figure 2a), $\sigma_{f_{obs}}$ as the error. For MAVEN data, $\sigma_{f_{obs}}$ is the propagated statistical error. For MEPA data, $\sigma_{f_{obs}}$ represents the system uncertainty and it equals to $f_{obs}\cdot\delta_{ins}$ with δ_{ins} corresponding to 46%, 36%, 24%, 29%, 52%, 16%, 14% for the selected 7 energy channels, respectively.
5. For each random $F_p(E_p)$ value derived from step 1–3 and random flux data $F_{ran} \sim N(f_{obs},\sigma_{f_{obs}}^2)$ generated within the measurement uncertainties, fit them with the following Band function:

$$F(E) = \begin{cases} f_0\left(\frac{E}{100\mathrm{KeV}}\right)^{-\gamma_1}\exp\left(-\frac{E}{E_0}\right), & E < (\gamma_2-\gamma_1)E_0 \equiv E_1 \\ f_0\left(\frac{E_1}{100\mathrm{KeV}}\right)^{-\gamma_1}\exp\left(-\frac{E_1}{E_0}\right)\left(\frac{E}{E_1}\right)^{-\gamma_2}, & E \geq E_1 \end{cases} \quad (5)$$

6. In order to account for uncertainties arising from different factors (see steps 1–4), the Band function is fitted to 10,000 spectra randomly generated as shown in steps 1–4, the results are depicted in Figure 2b.

In order to avoid unphysical results of the energy spectrum, we restrict the parameters of the band function to $\gamma_1 > 0$ and $\gamma_2 > \gamma_1$. The green dotted line represents the Band function utilizing four average parameters while the shaded area shows the percentage of 10,000 times of Band function fitting. Figure 2c additionally illustrates the distribution of the four parameters derived from 10,000 fits which generally follow a Gaussian distribution. Compared to the parameters of the Ground Level Enhancements (GLEs) list in Raukunen et al. (2018, Table 2), the power-law indices and break energy of this event ($\gamma_1 = 0.19, \gamma_2 = 2.97, E_0 = 23.4$ MeV) are smaller than those of the spectra of most GLEs reconstructed at Earth ($\bar{\gamma}_1 = 1.69, \bar{\gamma}_2 = 6.10, \bar{E}_0 = 100$ MeV which are averaged over all GLE events in that study). It is difficult to conclude whether this is due to propagation effect at different solar radial distances or this is a special feature of this individual event. More statistical analysis of SEP events at Mars and multi-spacecraft analysis of SEPs especially with observers located at close-by magnetic field lines and at different solar radial distances are essential to better understand this.

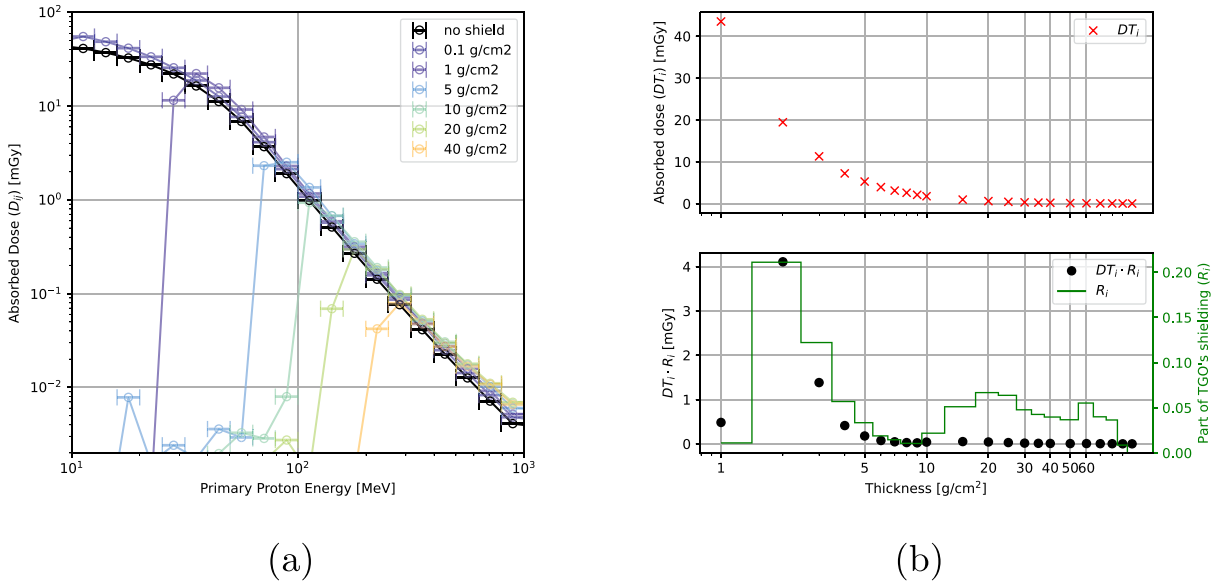

Figure 3. Modeling the event dose considering the shielding of TGO. (a) The simulated absorbed dose D_{ij} (y-axis) induced by primary protons with different primary energy E_j (x-axis) with the Al-shielding of various thicknesses T_i (see legend). (b) Upper panel: the absorbed dose induced by primary protons and their secondary particles after passing through different shielding thicknesses (red crosses). Lower panel: the distribution of TGO's shielding thickness (green stairs) and the corresponding absorbed dose considering the shielding distribution (black dots).

3. Modeling Radiation Dose Observed at Mars Orbit and Surface

3.1. From SEP Spectra to Dose in TGO/Liulin-MO

The shading effect of Mars on space radiation particle fluxes measured by the Liulin-MO instrument has been studied by Krastev et al. (2019) and Liu et al. (2023). Their results suggest that as the probe's orientation transitions from being tangent to Mars to directly facing Mars, the presence of Mars can cause a shielding effect resulting in a decrease in fluxes ranging from 23% to 40%. Different from the flux, it is important to note that the radiation dose detected within an isotropic field (where shielding, if exists, is also nearly isotropic) does not depend on the detector orientation. Thus, for dose calculations, we consider Mars as a solid body that shields away the SEPs coming from deep space. The shading coefficient can be calculated with $K_{sh} = \frac{1}{2} - \frac{1}{2}\cos\left(\arcsin\left(\frac{Mars\ radius}{Distance\ to\ Mars}\right)\right)$. Substituting the Mars radius of 3,390 km and the TGO's orbital altitude of 400 km into the formula, K_{sh} is ~0.28.

Nevertheless, particles arriving at Mars orbit need to go through certain spacecraft shielding before reaching TGO's Liulin-MO dosimeter detectors. The thickness of TGO's shield is highly non-uniform and ranges from ~1 g/cm^2 to ~70 g/cm^2 to aluminum equivalent shielding thickness (Figure 5 in Semkova et al., 2018). Direct simulation of particle transport through the TGO's shield using GEANT4 is highly complex as this requires a detailed 3D model of the TGO spacecraft. Alternatively, we use a fulfilled transport matrix, A_{ijk}, of protons penetrating aluminum spherical shells, each having thicknesses T_i, with an input energy E_j and an output energy E_k (Appel et al., 2018; Dobynde et al., 2021). For each given thickness, we calculated particle flux inside the shielding and then the absorbed dose induced by particles in a 300-micron thick silicon slab following this equation:

$$DET_{ij} = \sum_k A_{ijk} \cdot F_j \cdot \frac{LET(E_k)}{\rho} \cdot W_k, \tag{6}$$

where F_j is the fluence of the primary proton at energy E_j outside the shielding, LET (dE/dx) is the linear energy transfer in silicon, ρ is the density of silicon, W_k is the energy bin width of the output spectra.

Figure 3a shows the absorbed dose in silicon, DET_{ij}, caused by primary protons of different energies, E_j, when passing through various thicknesses. The absorbed dose will be cut off at lower energy levels as a result of

shielding, with the cut-off energy threshold rising with the shielding thickness. It is seen that the absorbed dose resulting from the primary protons with energies above the cut-off energy slightly increases as the shielding thickness increases. This is attributed to the secondary particles produced by the primary protons as they traverse the shielding material. The absorbed dose for cases of various shielding thicknesses, $DT_i = \sum_j DET_{ij}$, and the corresponding proportions in the TGO's shield, R_i, are shown in Figure 3b. Here the thickness of the TGO's shield is scaled to the simulated thickness as shown by the green line in the bottom panel. Finally, the results obtained from different shielding thicknesses are weighted according to the TGO thickness distribution around the detector to obtain the expected absorbed dose induced by the SEP event in the TGO radiation detector, $D = \sum_i R_i \cdot DT_i$ (shown as black dots in the bottom panel).

3.2. From Primary SEP Spectra to Surface Dose in MSL/RAD

Primary particles passing through the atmosphere may generate secondaries of different types and energies, so the surface dose is a result of the secondary particles generated by the primary SEPs. To get the particle spectra on Martian surface, a GEANT4-based planetary particle transport simulation tool named Atmospheric Radiation Interaction Simulator (AtRIS, Banjac et al., 2018) is utilized. AtRIS has been validated using particle flux measurements by MSL/RAD within the Gale crater by Guo, Banjac, et al. (2019) who also found that the FTFP_INCLXX_HP physics list is most suitable for Martian environment. The model represents Mars as a geometric sphere with a radius of 3,390 km, featuring a 100 m-thick crust composed of 50% Si, 40% O, and 10% Fe with a density of 1.79 g/cm2. The atmosphere above the surface is 80 km thick, with a density and composition profile sourced from the Mars Climate Database (MCD4.3, Millour et al., 2008, http://www-mars.lmd.jussieu.fr). The atmosphere is predominantly composed of CO_2, with other elements such as C, O, N, Ar, and H present. The surface pressure in this study is set to be 750 Pa. As a result of AtRIS, the conversion matrix B_{jk} that converts flux at input energy E_j into flux at output energy E_k can be utilized directly to compute the radiation D_R of this SEP event on the surface where RAD is located following Equation 7:

$$D_{surf} = \sum_{jk} B_{jk} \cdot F_j \cdot \frac{LET(E_k)}{\rho} \cdot W_k \tag{7}$$

Using approaches described in this section and the SEP spectra at Mars as derived in Section 2, we predicted dose in TGO/Liulin-MO to be 6.94 ± 0.73 mGy, about 23% larger than the measured of 5.66 mGy during the selected 12 hr window. The predicted dose in RAD silicon detector "B" is 0.290 ± 0.065 mGy, also slightly larger than the measured 0.248 mGy by approximately 17% during the 12 hr interval. Note that for the whole event, the absorbed dose measured by TGO/Liulin-MO is about 13.8 mGy (Semkova et al., 2023) and by RAD silicon detector "B" is about 0.365 mGy. Various factors may result in this discrepancy between modeled and measured doses, which will be discussed in the next section.

4. Summary and Discussion

We present the observations by different spacecraft during the SEP event on 15–16 February 2022 and focus on deriving the SEP proton flux and associated radiation exposure both on the surface and in orbit of Mars. We carry out synergistic analysis of the SEP event combining particle flux and radiation dose detectors from different missions, including the Chinese TW-1, ESA's TGO, and NASA's MSL and MAVEN missions. In particular and for the first time, we show the Chinese TW-1/MEPA's observation of high-energy proton flux at Mars orbit. With its capability to detect protons up to 100 MeV, MEPA complements MAVEN for detecting protons with critical radiation risks at Mars orbit and makes a large step forward for assessing the radiation environment near Mars. However, for evaluating the Martian surface radiation environment, we still need in-situ observations provided by MSL/RAD since most lower-energy (<150 MeV) protons can not reach the surface.

The high-energy protons in this event penetrated the Martian atmosphere and induced radiation enhancement on the surface. The absorbed dose measured by the RAD detector allows us to derive the primary flux of the protons at about 300 MeV according to the pivot-energy method for the radiation environment on Mars (Guo, Wimmer-Schweingruber et al., 2019). Besides, the TW-1 spacecraft carrying the MEPA detector makes it possible to directly detect protons up to about 100 MeV and fills up the critical gap in which the break energy of the SEP double power-law spectrum normally locates (Raukunen et al., 2018). Combining the observed proton flux of 1–

6 MeV by MAVEN and 20–100 MeV by MEPA with the derived proton flux at about 300 MeV from the surface RAD measurement, we reconstruct the SEP event spectrum using the Band function as shown in Section 2.

To further validate the reconstructed spectrum, we use it to calculate the expected radiation dose as observed by the TGO/Liulin-MO orbiting Mars and by the MSL/RAD on the surface. Despite the relatively broad and simplified approach of the detector modeling (Section 3), the eventual result — full chain of SEP spectra reconstruction and the derived radiation dose — is quite satisfactory as compared to observations. In either orbital or surface cases, the discrepancy between measured and simulated dose results is less than 25%, which to a certain extent (compared to the measurement errors given in item four in Section 2.3) validates the reliability of the reconstructed proton spectra and the measurements involved in this study (energetic particle data from TW-1, MAVEN, MSL and TGO).

Various factors may result in this discrepancy. For instance, the 1 GeV high-energy cutoff of the event might be an overestimate, causing the simulated doses to include more high-energy particles than the actual event; the simplification of the TGO shielding model may underestimate the actual shielding effect, causing the simulated doses to consider more low-energy particles that should have been shielded; the actual RAD detector and MSL rover structure may provide further shielding of the surface radiation which is not yet included in the Mars atmospheric transport modeling (although we adopt the second top "B" detector, we did not account for shielding by the top "A" detector and by spacecraft materials, especially for particles coming at large zenith angles). The most important factor is probably the lack of data coverage in different energies and directions. As detailed in Section 2.2, the proton flux at the pivot energy is derived from surface MSL/RAD that was preferentially detecting particles from the Sun during the main phase of this event. Since SEPs from the Solar direction normally have a larger flux during the early phase of SEP events, the pivot-energy derived flux may be larger than the flux averaged out over different directions which was contributing to the TGO measurement (TGO has an orbital period of about 2 hr and the directionality effect can be ignored in the dose recorded in the 12 hr window.)

Overall, our result shows that the proton flux measurement by TW-1/MEPA and the derivation of ∼300 MeV proton flux from MSL/RAD in synergy provide a much more complete assessment of the radiation environment at Mars, especially for large SEP events comprising high-energy protons (above tens of MeV). However, better coverage of data over different energies and directions both at the orbit and surface of Mars will further improve the accuracy of the assessment of the Martian radiation environment. Combining all available particle and radiation detectors at Mars together with the state-of-the-art Mars radiation environment models, our study emphasizes the necessity of continuous and synergistic radiation monitoring at Mars.

Data Availability Statement

We acknowledge the following data sources: TGO/Liulin-MO (http://esa-pro.space.bas.bg/datasources), MSL/RAD and MSL/REMS from NASA planetary data systems (https://pds-ppi.igpp.ucla.edu/collection/MSL-M-RAD-2-EDR-V1.0:CALIBRATION for RAD; https://atmos.nmsu.edu/PDS/data/mslrem_1001/DATA/ for REMS), MAVEN from Coordinated Data Analysis Web (https://cdaweb.gsfc.nasa.gov) and TW-1 mission data provided by the China National Space Administration (CNSA, https://moon.bao.ac.cn/). The AtRIS code used to model the Martian radiation environment is uploaded at Zenodo platform (Banjac, 2019).

Acknowledgments
We thank the two reviewers for their helpful review and we thank Rob Lillis and Christina Lee from the MAVEN team for their advice on the MAVEN data usage. We thank Cary Zeitlin for the help with the MSL/REMS data. We acknowledge the Key Research Program and the Strategic Priority Program of the Chinese Academy of Sciences (Grant ZDBS-SSW-TLC00103, XDB41000000) and the National Natural Science Foundation of China (42188101, 42074222 and 42130204). RAD is supported by NASA (HEOMD) under JPL subcontract 1273039 to Southwest Research Institute, and in Germany by the German space Agency (50QM0501, 50QM1201, and 50QM1701) to the Christian Albrechts University, Kiel.

References

Appel, J. K., Köhler, J., Guo, J., Ehresmann, B., Zeitlin, C., Matthiä, D., et al. (2018). Detecting upward directed charged particle fluxes in the mars science laboratory radiation assessment detector. *Earth and Space Science*, *5*(1), 2–18. https://doi.org/10.1002/2016EA000240

Band, D., Matteson, J., Ford, L., Schaefer, B., Palmer, D., Teegarden, B., et al. (1993). Batse observations of gamma-ray burst spectra. i-spectral diversity. *The Astrophysical Journal*, *413*, 281–292. https://doi.org/10.1086/172995

Banjac, S. (2019). Atmospheric radiation interaction simulator (AtRIS) [Software]. *Zenodo*. Retrieved from https://doi.org/10.5281/zenodo.3633451

Banjac, S., Herbst, K., & Heber, B. (2018). The atmospheric radiation interaction simulator (AtRIS) - Description and validation. *Journal of Geophysical Research: Space Physics*, *123*(ja), 50–67. https://doi.org/10.1029/2018JA026042

Dobynde, M., Shprits, Y., Drozdov, A., Hoffman, J., & Li, J. (2021). Beating 1 Sievert: Optimal radiation shielding of astronauts on a mission to mars. *Space Weather*, *19*(9), e2021SW002749. https://doi.org/10.1029/2021SW002749

Dumbović, M., Guo, J., Temmer, M., Mays, M. L., Veronig, A., Heinemann, S. G., et al. (2019). Unusual plasma and particle signatures at Mars and stereo-a related to cme–cme interaction. *The Astrophysical Journal*, *880*(1), 18. https://doi.org/10.3847/1538-4357/ab27ca

Fu, S., Ding, Z., Zhang, Y., Zhang, X., Li, C., Li, G., et al. (2022). First report of a solar energetic particle event observed by China's tianwen-1 mission in transit to mars. *The Astrophysical Journal Letters*, *934*(1), L15. https://doi.org/10.3847/2041-8213/ac80f5

Gieseler, J., Dresing, N., Palmroos, C., Freiherr von Forstner, J. L., Price, D. J., Vainio, R., et al. (2023). Solar-mach: An open-source tool to analyze solar magnetic connection configurations. *Frontiers in Astronomy and Space Sciences*, *9*, 1058810. https://doi.org/10.3389/fspas.2022.1058810

Grotzinger, J. P., Crisp, J., Vasavada, A. R., Anderson, R. C., Baker, C. J., Barry, R., et al. (2012). Mars Science Laboratory mission and science investigation. *Space Science Reviews*, *170*(1), 5–56. https://doi.org/10.1007/s11214-012-9892-2

Guo, J., Banjac, S., Röstel, L., Terasa, J. C., Herbst, K., Heber, B., & Wimmer-Schweingruber, R. F. (2019a). Implementation and validation of the GEANT4/AtRIS code to model the radiation environment at Mars. *Journal of Space Weather and Space Climate*, *9*(A2), A7. https://doi.org/10.1051/swsc/2019004

Guo, J., Wimmer-Schweingruber, R. F., Wang, Y., Grande, M., Matthiä, D., Zeitlin, C., et al. (2019b). The pivot energy of solar energetic particles affecting the martian surface radiation environment. *The Astrophysical Journal Letters*, *883*(1), L12. https://doi.org/10.3847/2041-8213/ab3ec2

Guo, J., Zeitlin, C., Wimmer-Schweingruber, R. F., Hassler, D. M., Ehresmann, B., Rafkin, S., et al. (2021). Radiation environment for future human exploration on the surface of mars: The current understanding based on MSL/RAD dose measurements. *aapr*, *29*(1), 8. https://doi.org/10.1007/s00159-021-00136-5

Guo, J., Zeitlin, C., Wimmer-Schweingruber, R. F., McDole, T., Kā¼hl, P., Appel, J. C., et al. (2018). A generalized approach to model the spectra and radiation dose rate of solar particle events on the surface of Mars. *The Astronomical Journal*, *155*(1), 49. https://doi.org/10.3847/1538-3881/aaa085

Hassler, D. M., Zeitlin, C., Wimmer-Schweingruber, R. F., Böttcher, S. I., Martin, C., Andrews, J., et al. (2012). The radiation assessment detector (RAD) investigation. *Space Science Reviews*, *170*(1), 503–558. https://doi.org/10.1007/s11214-012-9913-1

Hassler, D. M., Zeitlin, C., Wimmer-Schweingruber, R. F., Ehresmann, B., Rafkin, S., Eigenbrode, J. L., et al. (2014). Mars's surface radiation environment measured with the Mars Science Laboratory's curiosity rover. *Science*, *343*(6169), 1244797. https://doi.org/10.1126/science.1244797

Khoo, L., Sánchez-Cano, B., Lee, C., Rodríguez-García, L., Kouloumvakos, A., Palmerio, E., et al. (2024). Multispacecraft observations of a widespread solar energetic particle event on 2022 february 15–16. *The Astrophysical Journal*, *963*(2), 107. https://doi.org/10.3847/1538-4357/ad167f

Krastev, K., Semkova, J., Koleva, R., Bankov, N., Benghin, V., & Drobishev, S. (2019). The shading effect on galactic cosmic rays fluxes and doses measured by liulin-mo instrument on near-mars orbit. eleventh workshop 'solar influences on the magnetosphere, ionosphere and atmosphere. In *Book of proceedings* (pp. 31–34). https://doi.org/10.31401/WS.2019.proc

Larson, D. E., Lillis, R. J., Lee, C. O., Dunn, P. A., Hatch, K., Robinson, M., et al. (2015). The maven solar energetic particle investigation. *Space Science Reviews*, *195*(1–4), 153–172. https://doi.org/10.1007/s11214-015-0218-z

Lee, C., Hara, T., Halekas, J., Thiemann, E., Chamberlin, P., Eparvier, F., et al. (2017). Maven observations of the solar cycle 24 space weather conditions at Mars. *Journal of Geophysical Research: Space Physics*, *122*(3), 2768–2794. https://doi.org/10.1002/2016JA023495

Li, C., Tang, S., Hu, X., Qian, Y., Wang, Y., Zhao, H., et al. (2021). Design and realization of China tianwen-1 energetic particle analyzer. *Space Science Reviews*, *217*(2), 1–20. https://doi.org/10.1007/s11214-021-00803-0

Liu, W., Guo, J., Zhang, J., & Semkova, J. (2023). Modeling the radiation environment of energetic particles at mars orbit and a first validation against tgo measurements. *The Astrophysical Journal*, *949*(2), 77. https://doi.org/10.3847/1538-4357/acce3c

Millour, E., Forget, F., & Lewis, S. (2008). Mars climate database v4. 3 detailed design document. Available on http://web.lmd.jussieu.fr/forget/dvd/docs

Mishev, A., & Usoskin, I. (2019). Analysis of sub-gle and gle events using nm data: Space weather applications. *Journal of Physics: Conference Series*, *1181*, 012006. https://doi.org/10.1088/1742-6596/1181/1/012006

Raukunen, O., Vainio, R., Tylka, A. J., Dietrich, W. F., Jiggens, P., Heynderickx, D., et al. (2018). Two solar proton fluence models based on ground level enhancement observations. *Journal of Space Weather and Space Climate*, *8*, A04. https://doi.org/10.1051/swsc/2017031

Semkova, J., Benghin, V., Guo, J., Zhang, J., Da Pieve, F., Krastev, K., et al. (2022). Comparison of the flux measured by liulin-mo dosimeter in exomars tgo science orbit with the calculations. *Life Sciences and Space Research*, *39*, 119–130. https://doi.org/10.1016/j.lssr.2022.08.007

Semkova, J., Koleva, R., Benghin, V., Dachev, T., Matviichuk, Y., Tomov, B., et al. (2021). Results from radiation environment measurements aboard exomars trace gas orbiter in mars science orbit in may 2018–december 2019. *Icarus*, *361*, 114264. https://doi.org/10.1016/j.icarus.2020.114264

Semkova, J., Koleva, R., Benghin, V., Dachev, T., Matviichuk, Y., Tomov, B., et al. (2018). Charged particles radiation measurements with liulin-mo dosimeter of frend instrument aboard exomars trace gas orbiter during the transit and in high elliptic mars orbit. *Icarus*, *303*, 53–66. https://doi.org/10.1016/j.icarus.2017.12.034

Semkova, J., Koleva, R., Benghin, V., Krastev, K., Matviichuk, Y., Tomov, B., et al. (2023). Observation of the radiation environment and solar energetic particle events in mars orbit in may 2018-june 2022. *Life Sciences and Space Research*, *39*, 106–118. https://doi.org/10.1016/j.lssr.2023.03.006

Tang, S., Wang, Y., Zhao, H., Fang, F., Qian, Y., Zhang, Y., et al. (2020). Calibration of mars energetic particle analyzer (MEPA). *Earth and Planetary Physics*, *4*(4), 355–363. https://doi.org/10.26464/epp2020055

Thernisien, A. (2011). Implementation of the graduated cylindrical shell model for the three-dimensional reconstruction of coronal mass ejections. *The Astrophysical Journal - Supplement Series*, *194*(2), 33. https://doi.org/10.1088/0067-0049/194/2/33

Zeitlin, C., Hassler, D. M., Cucinotta, F. A., Ehresmann, B., Wimmer-Schweingruber, R. F., Brinza, D. E., et al. (2013). Measurements of energetic particle radiation in transit to mars on the mars science laboratory. *Science*, *340*(6136), 1080–1084. https://doi.org/10.1126/science.1235989

Zhang, J., Guo, J., & Dobynde, M. I. (2023). What is the radiation impact of extreme solar energetic particle events on mars? *Space Weather*, *21*(6), e2023SW003490. https://doi.org/10.1029/2023SW003490